

Supporting Information for

“Si(bzimpy)₂ – A Hexacoordinate Silicon Pincer Complex for Electron Transport and Electroluminescence”

Margaret Kocherga,^a Jose Castaneda,^b Michael G. Walter,^a Yong Zhang,^b Nemah-Allah Saleh,^a Le Wang,^a Daniel S. Jones,^a Jon Merkert,^a Bernadette Donovan-Merkert,^a Yanzeng Li,^c Tino Hofmann,^c and Thomas A. Schmedake^{a,*}

Table of Contents

<i>Instrumentation and synthetic details</i>	2 – 4
<i>Mass spectrometry and NMR spectra</i>	5 – 11
<i>TGA and FTIR</i>	12 – 13
<i>Fluorescence properties in solid state</i>	14
<i>Fluorescence properties in mixed solutions</i>	15
<i>Computational modeling</i>	16 – 18
<i>Cyclic voltammogram</i>	19
<i>J-V curves and electron mobility data</i>	20
<i>References</i>	21

^a University of North Carolina - Charlotte, Department of Chemistry, Charlotte, NC 28223, USA

^b University of North Carolina - Charlotte, Department of Electrical and Computer Engineering, Charlotte, NC 28223, USA

^c University of North Carolina - Charlotte, Department of Physics and Optical Science, Charlotte, NC 28223, USA

*Email: Tom.Schmedake@unc Charlotte.edu

Experimental

Instrumentation and General Methods

Absorption spectra were measured with a Cary 300 UV-Vis spectrophotometer. Fluorescence measurements were conducted on a Jobin-Yvon Fluorolog 3 fluorescence spectrometer. NMR spectra were acquired using a JEOL 500 MHz NMR spectrometer. Combustion analysis (C, H, and N) was conducted by Atlantic Microlab, Inc. IR spectra were recorded on pure solids on a Perkin-Elmer Spectrum100 FT-IR spectrometer and are reported in cm^{-1} ; relative intensities of the absorptions are indicated in parentheses (vs = very strong, s = strong, m = medium, w = weak). Thermogravimetric analysis was performed using Mettler Toledo TGA/SDTA851 instrument (Mettler-Toledo AG Analytical, Schwerenbach, Switzerland). Mass spectrometry was performed using Voyager DE MALDI-TOF Mass Spectrometer

Cyclic voltammetry studies were performed using a Princeton Applied Research Model 273A Potentiostat/Galvanostat employing a conventional three-electrode setup consisting of a platinum working electrode, a silver/silver chloride reference electrode, and a platinum wire auxiliary electrode. Positive feedback iR compensation was routinely used. Voltammograms were obtained in 0.1 M tetrabutylammonium hexafluorophosphate (TBAPF_6)/acetonitrile solution using solvent that had previously been purified and dried using a solvent purification system (SPS- 400, Innovative Technologies) and subsequently purged with nitrogen. The supporting electrolyte (TBAPF_6) was recrystallized from ethanol and dried under vacuum prior to use. Ferrocene was used as an internal standard without further purification.

X-ray crystallography data were acquired with an Agilent (now Rigaku) Gemini A Ultra diffractometer. Crystals of suitable size were coated with a thin layer of paratone-N oil, mounted on the diffractometer, and flash cooled to 105 K in the cold stream of the Cryojet XL liquid nitrogen cooling device (Oxford Instruments) attached to the diffractometer. The diffractometer was equipped with sealed-tube long fine focus X-ray sources with Mo target ($\lambda = 0.71073 \text{ \AA}$) and Cu target ($\lambda = 1.5418 \text{ \AA}$), four-circle kappa goniometer, and CCD detector. CrysAlisPro¹ software was used to control the diffractometer and perform data reduction. The crystal structure was solved with SHELXS.² All non-hydrogen atoms appeared in the E-map of the correct solution. Alternate cycles of model-building in Olex2³ and refinement in SHELXL² followed. All non-hydrogen atoms were refined anisotropically. All hydrogen atom positions were calculated based on idealized geometry and recalculated after each cycle of least squares. During refinement, hydrogen atom – parent atom vectors were held fixed (riding motion constraint).

The surface roughness was investigated using a Dimension 3100 SPM System with NanoScope IV Controller Nanoman AFM. The film thickness was determined using a J. A. Woollam 6460LV VASE ellipsometer. A four phase model composed of glass substrate, substrate/film intermix, Si(bzimpy)₂, and air ambient was used for the data analysis. The parameterized model dielectric function of Si(bzimpy)₂ consisted of a Tauc-Lorentz oscillator in combination with two Lorentz oscillators. The dielectric function of the glass substrate was determined in a separate ellipsometric measurement.

Photoluminescence imaging was done by coupling a Kimmon 442 nm IK Series He-Cd laser into a Horiba LabRam HR800 Raman microscope equipped with a thermoelectrically cooled Synapse CCD. Laser excitation was focused onto films by use of an Olympus 100x MPlan N objective lens (0.9 NA) with a diffraction limited spot size of ~0.6 μm at a power density of ~0.4 kW/cm². Intensity images were produced by measuring photoluminescence in the range from 500 - 600 nm at a 0.1 second integration time with a 2.5 μm step between each pixel.

Synthesis of Si(bzimpy)₂

Under a nitrogen atmosphere, 2,6-bis(benzimidazol-2'-yl)pyridine (2.036 g, 6.5 mmol) in chloroform (60 mL) was stirred at 0 °C, and triethylamine was added to a stirring suspension (1.81 mL, 13.0 mmol). Upon addition of silicon tetrachloride (0.37 mL, 3.2 mmol) the mixture instantly turned yellow and was allowed to stir for 3 min at 0 °C. The resulting brownish-yellow suspension was warmed to room temperature, and the reaction allowed to proceed for 16 h with no stirring. The yellow solid obtained was separated by filtration, washed with chloroform (2 x 15 mL), and dried *in vacuo* for 1 h at 120 °C. The product was then suspended in acetone (60 mL), stirred for 1 h, and filtered to yield a bright yellow powder (1.170 g, 56%). The powder was purified further using Soxhlet extraction (0.100 g of Si(bzimpy)₂ was extracted with chloroform (350 mL)). The yellow luminescent solution was concentrated to dryness to obtain 0.068 g of product. (38% yield overall from SiCl₄). ¹H NMR(CD₂Cl₂, 500 MHz): δ 5.75 [d, J_{H-H} = 8.6, 4 H], 6.98 [dd, 4 H], 7.07 [dd, 4 H], 7.60 [d, J_{H-H} = 8.3, 4 H], 8.91 [m, 4 H], 8.99 [t, J_{H-H} = 7.8, 2 H]. ¹³C{¹H} NMR(CDCl₃/CD₃OD, 40/60 mixture, 125 MHz): δ 110.6, 119.9, 120.6, 123.5, 125.7, 134.9, 145.7, 147.3, 147.4, 150.4. ²⁹Si NMR(CDCl₃/CD₃OD, Cr(acac)₃ added, 40/60 mixture, 99 MHz): δ -185.7. IR data: 3400 (w), 3058 (w), 1629 (m), 1574 (m), 1558 (m), 1537 (w), 1473 (vs), 1438 (w), 1412 (w), 1376 (w), 1352 (m), 1322 (s), 1294 (w), 1263 (w), 1238 (w), 1194 (w), 1175 (w), 1146 (m), 1122 (w), 1089 (w), 1043 (m), 1007 (w), 963 (w), 926 (m), 835 (w), 816 (w), 807 (w), 738 (vs), 718 (m), 697 (w). Anal. Calc. for C₃₈H₂₂N₁₀Si·H₂O: C, 68.7; H, 3.6; N, 21.1. Found: C, 68.8; H, 3.9; N, 20.9%. MS (MALDI-TOF): m/z = 647.8.

Si(bzimp_y)₂ film growth and device fabrication:

Films were deposited using MB-EVAP with an integrated thermal deposition system inside an MBRAUN glovebox under high vacuum (10^{-6} mbar). The deposition of the films was controlled using a SQC-310C DepositionController. The evaporation of compound was done using a tungsten boat at the rate of 0.5-0.8 Å/s. The distance from the source to the film was 28 cm; the substrate holder was rotating at the speed 15 rpm. The area of the devices was found to be 2.94 mm². The OLED devices were fabricated on Pixelated Anode (6 pixel) ITO glass OLED substrates from Ossila. The ITO substrates were sonicated in acetone (15 min), then in isopropanol (15 min), and dried with nitrogen. The ITO patterned slides were treated in a UV/ozone ProCleaner for 20 min prior to being brought into the glovebox.

Electron mobility devices were prepared via deposition of 64 nm of Si(bzimp_y)₂, the thickness of which was confirmed via ellipsometry; followed by deposition of 300 nm of aluminum, the thickness of which was monitored using an Inficon quartz crystal monitor.

To assemble an OLED device, 78 nm of Si(bzimp_y)₂ was deposited onto an ITO patterned substrate, followed by deposition of 300 nm of aluminum. The thickness of both layers was monitored using an Inficon quartz crystal monitor.

A Keithley 236 source measure unit was used to apply the electric potential.

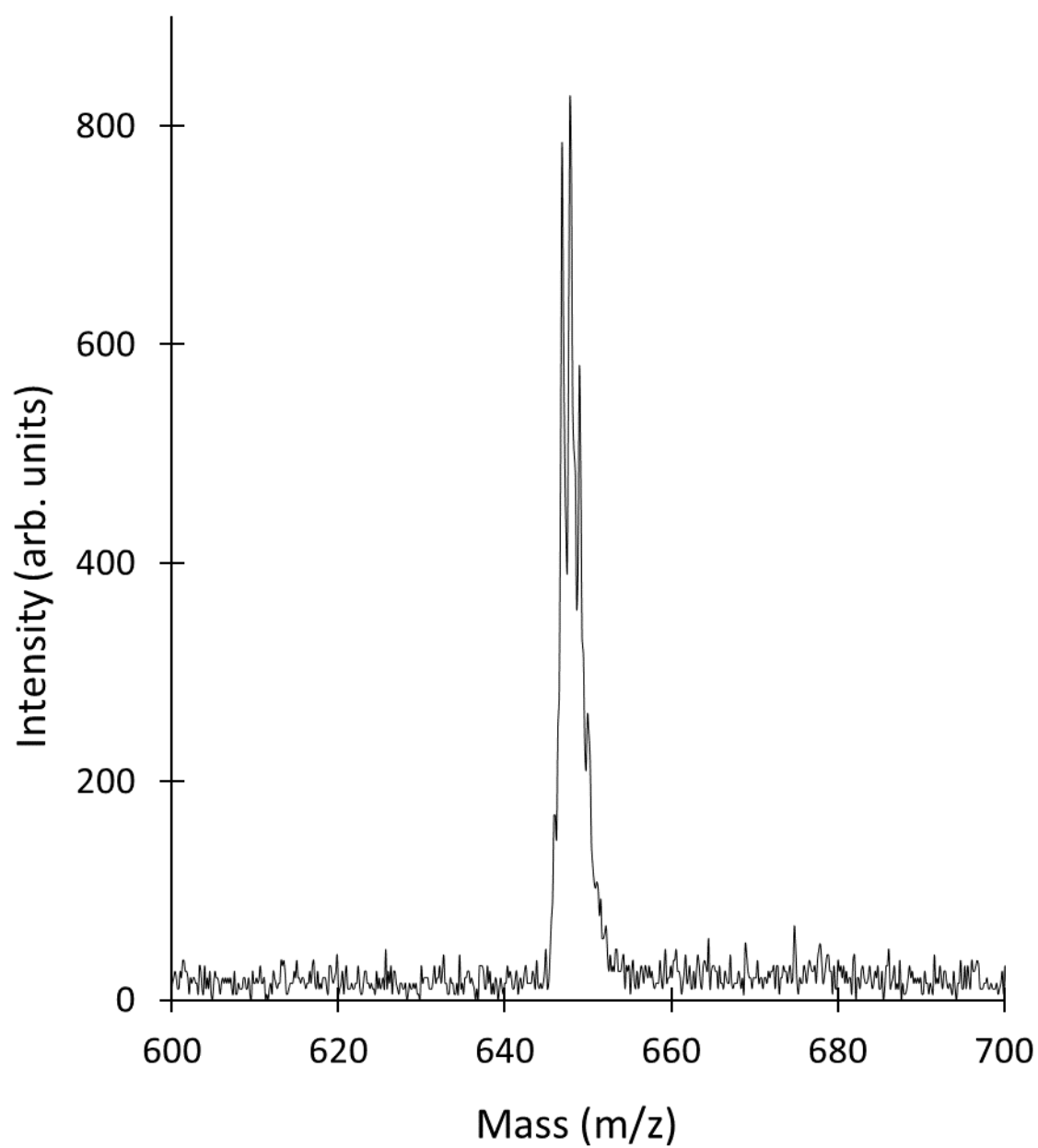


Figure S1. MALDI-TOF-MS spectrum of $\text{Si}(\text{bzimpy})_2$ (Matrix = 1,8,9-trihydroxyanthracene)

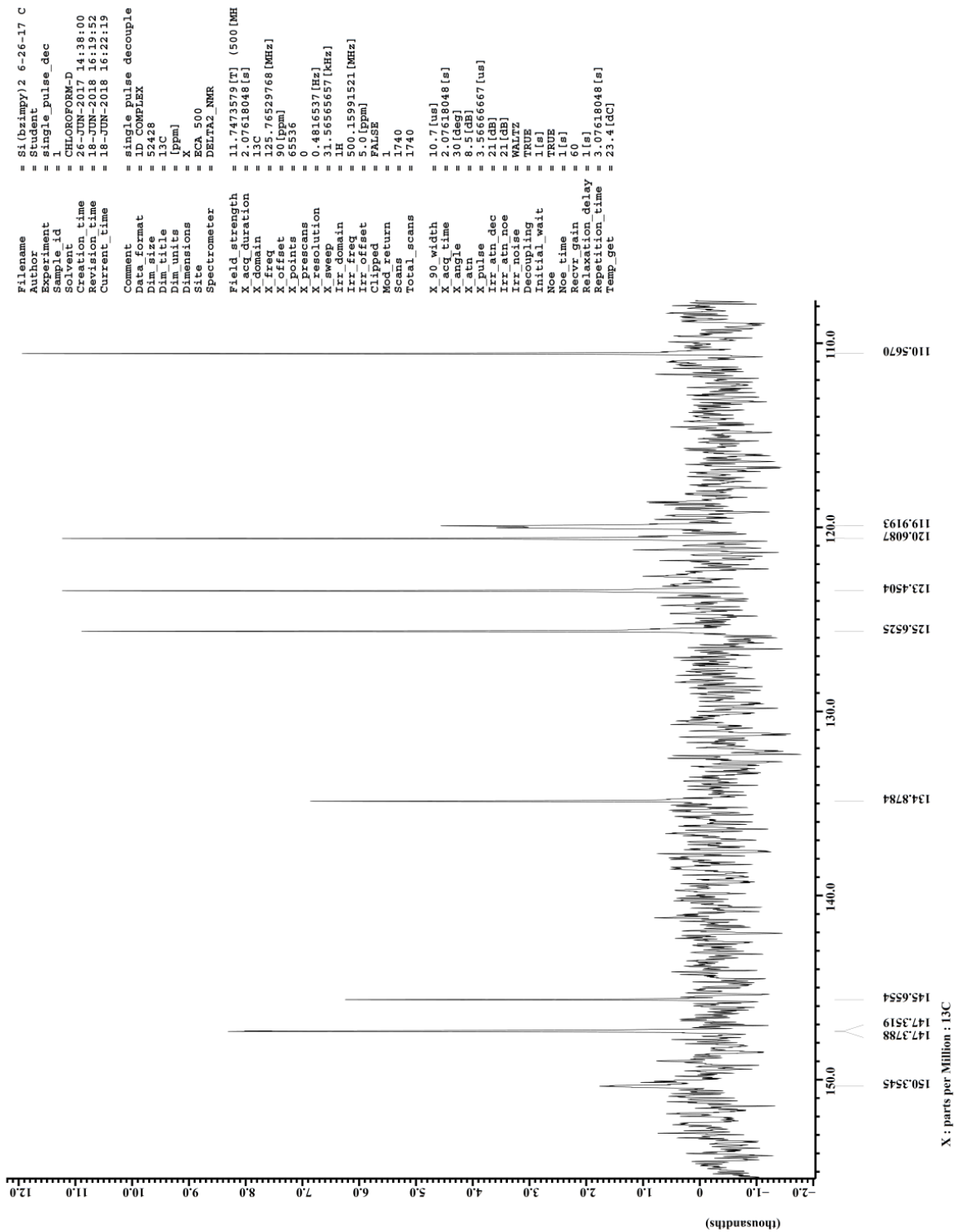


Figure S3. ^{13}C NMR spectrum of **Si(bzimpy)₂**. (125 Mhz, $\text{CDCl}_3/\text{CD}_3\text{OD}$)

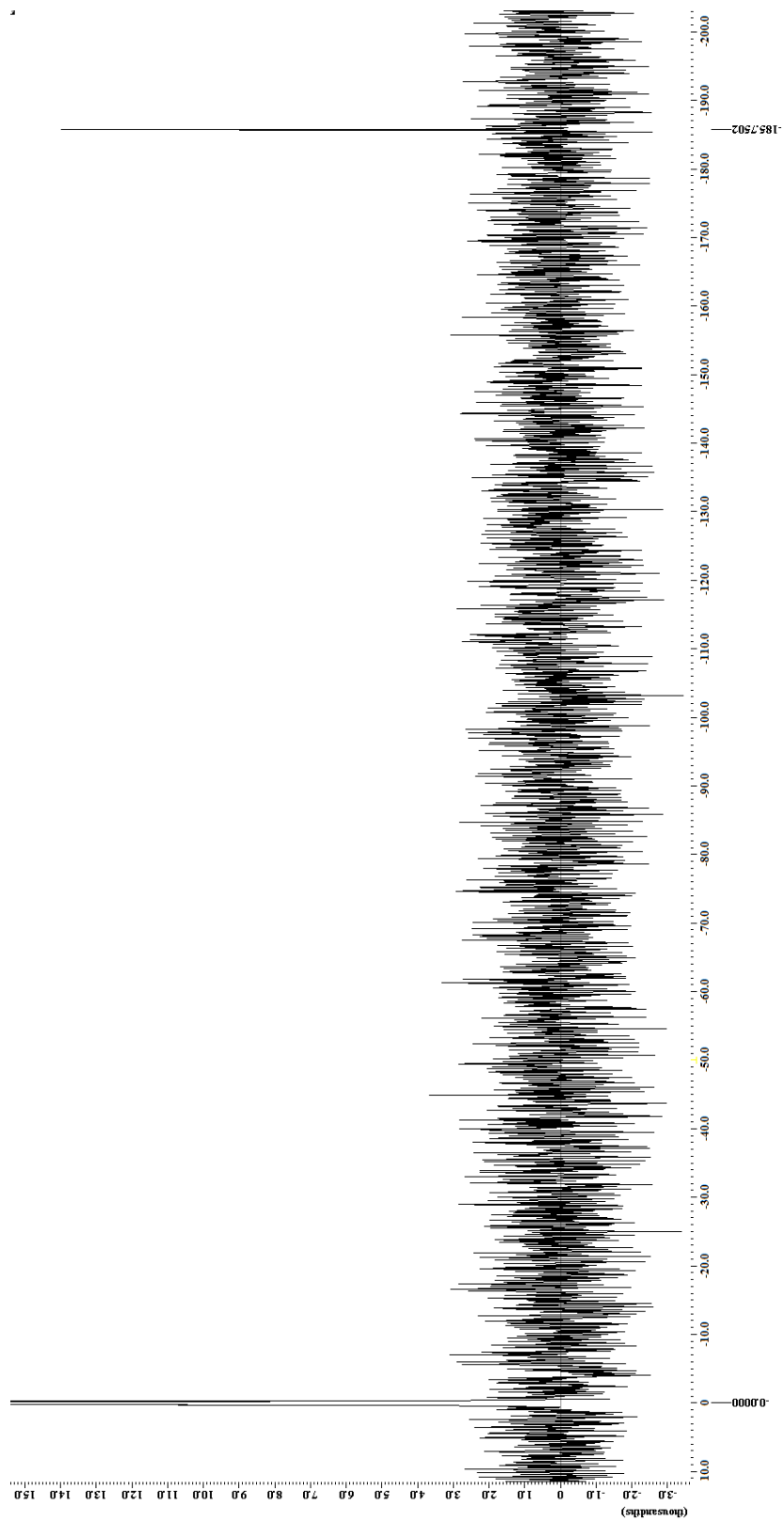


Figure S4. ^{29}Si NMR spectrum of **Si(bzimpy)₂**. (99 Mhz, $\text{CDCl}_3/\text{CD}_3\text{OD}$)

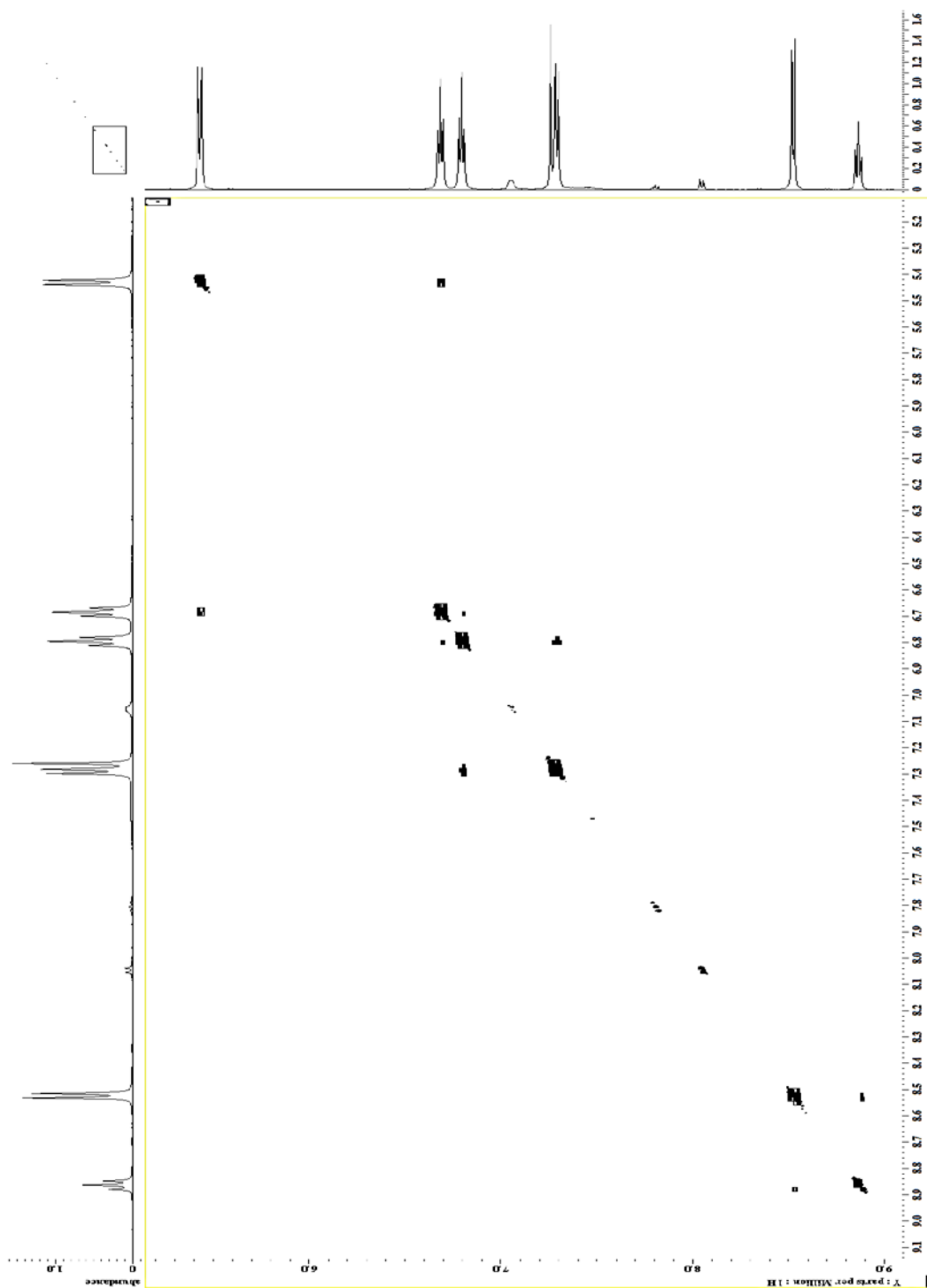


Figure S5. COSY NMR spectrum of **Si(bzimpy)₂**. (CDCl₃/CD₃OD)

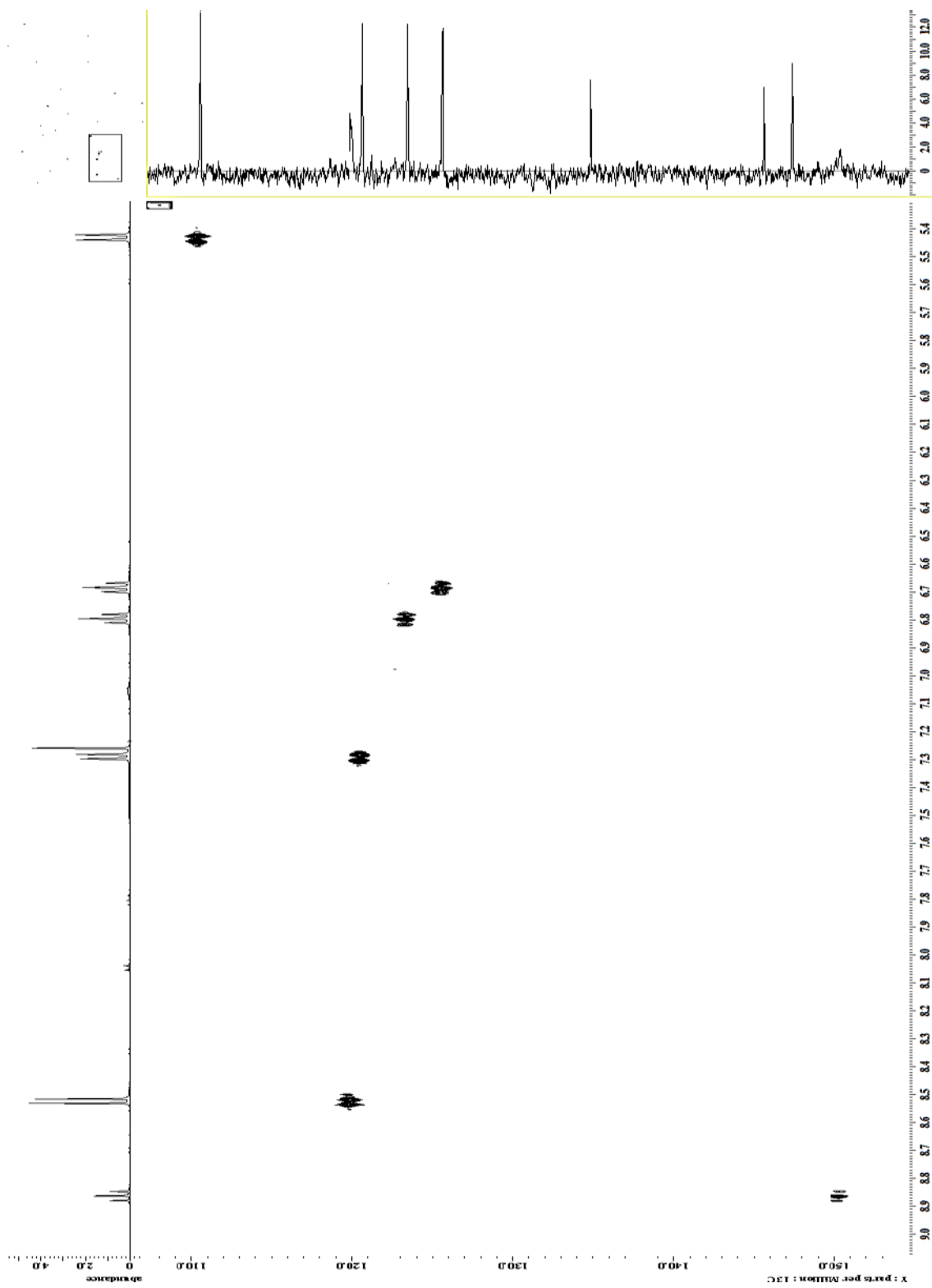
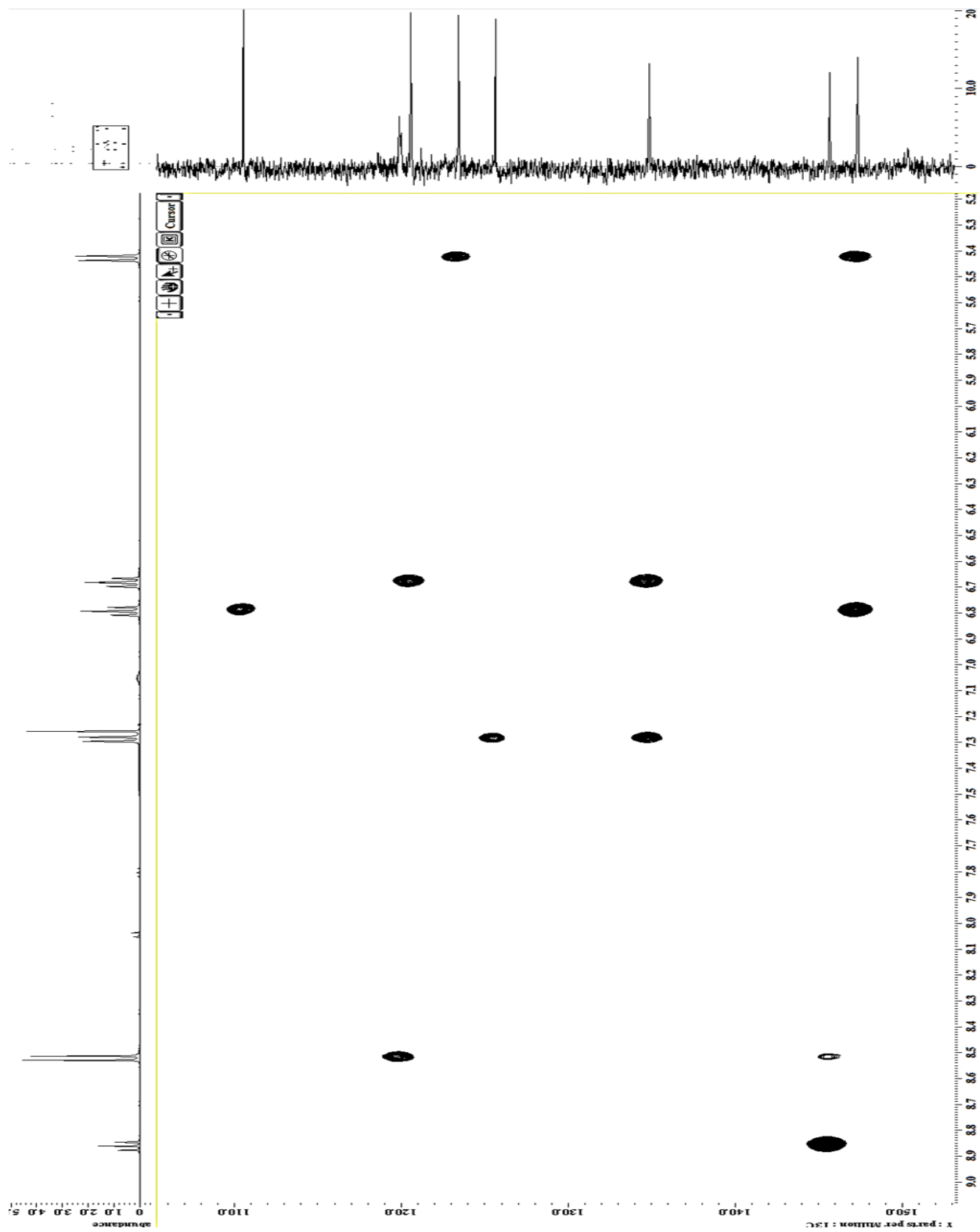


Figure S6. HMQC NMR spectrum of $\text{Si}(\text{bzimpy})_2$. ($\text{CDCl}_3/\text{CD}_3\text{OD}$)



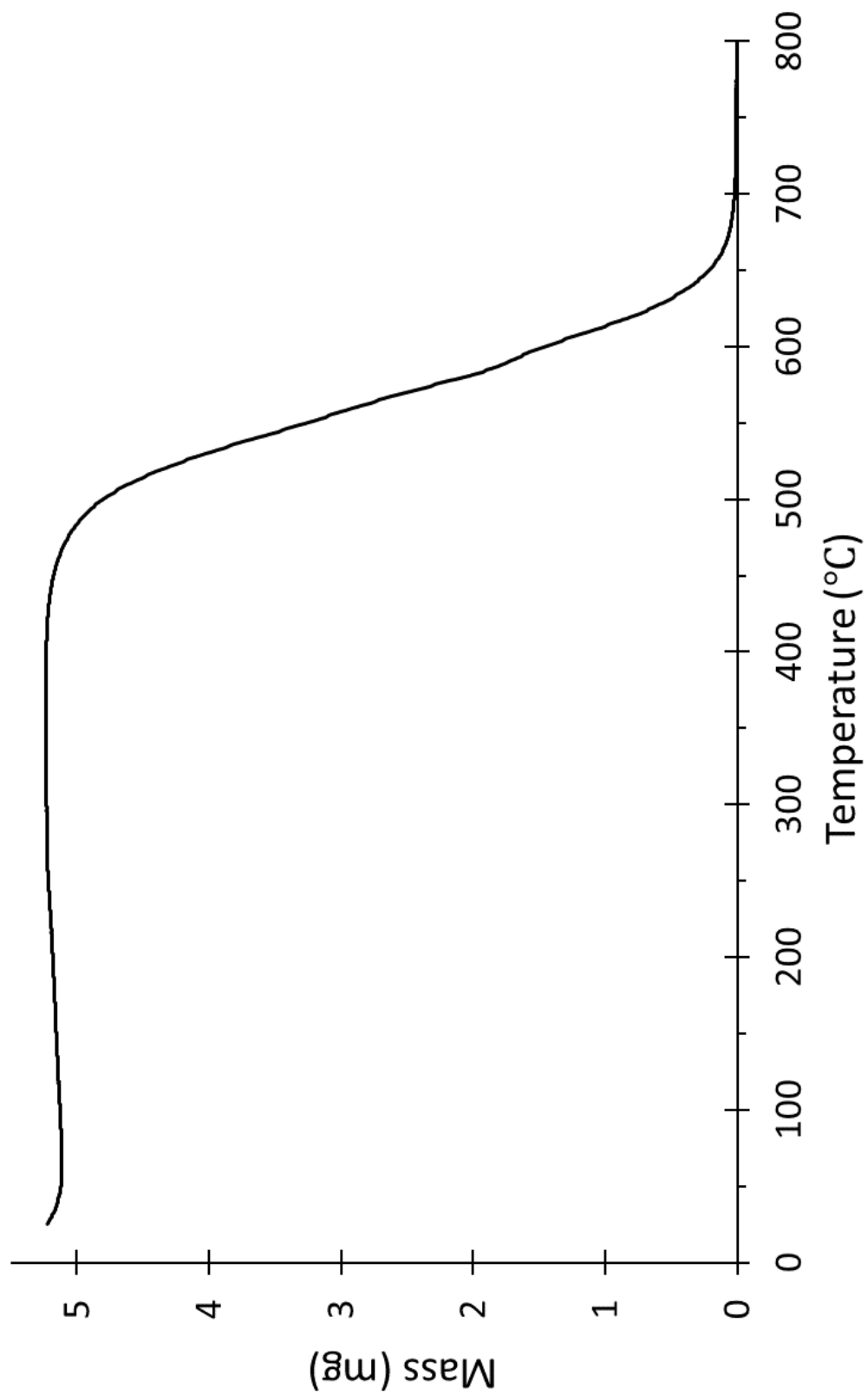


Figure S8. TGA of Si(bzimpy)₂.

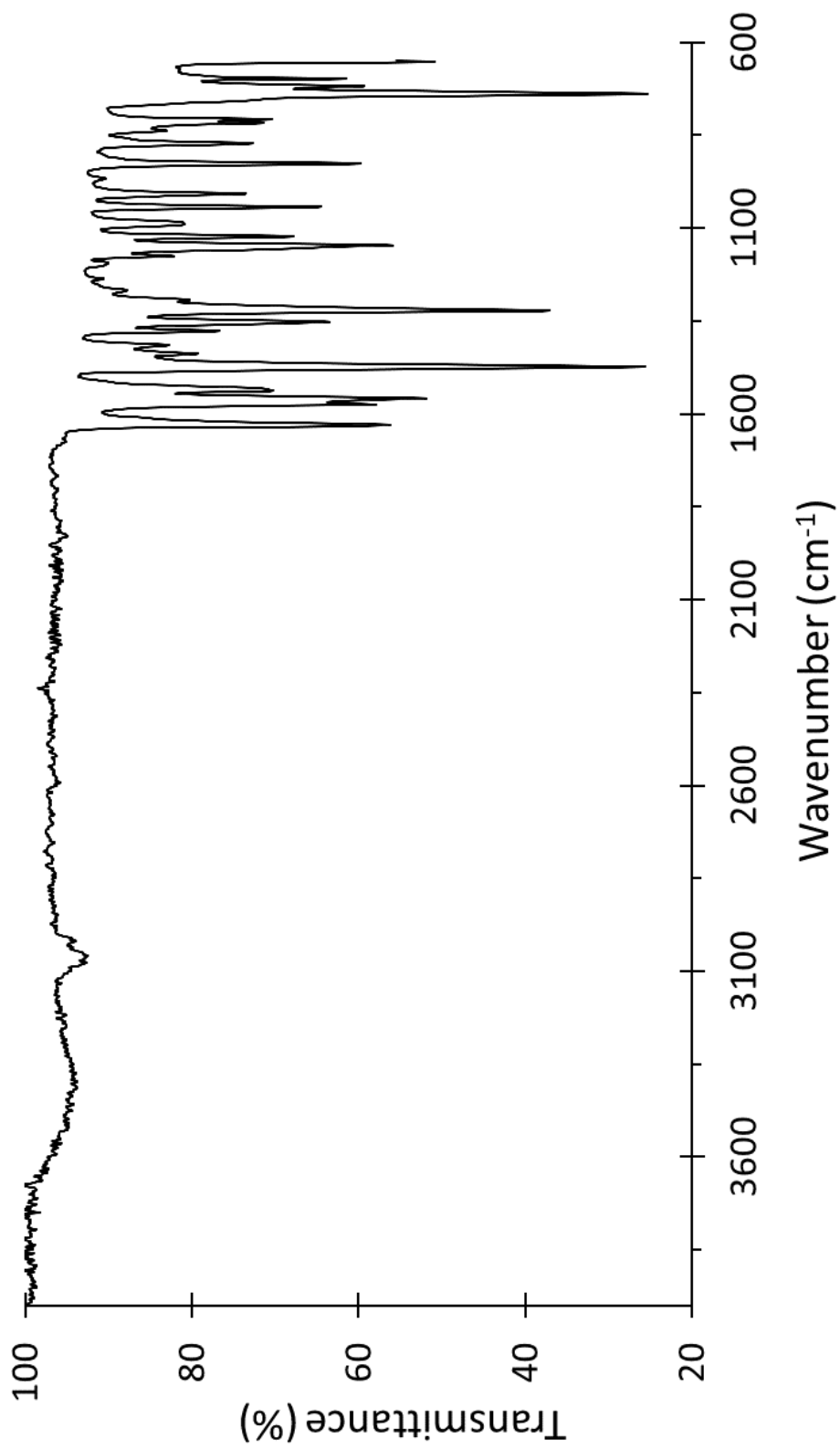


Figure S9. FTIR spectrum of Si(bzimpy)₂.

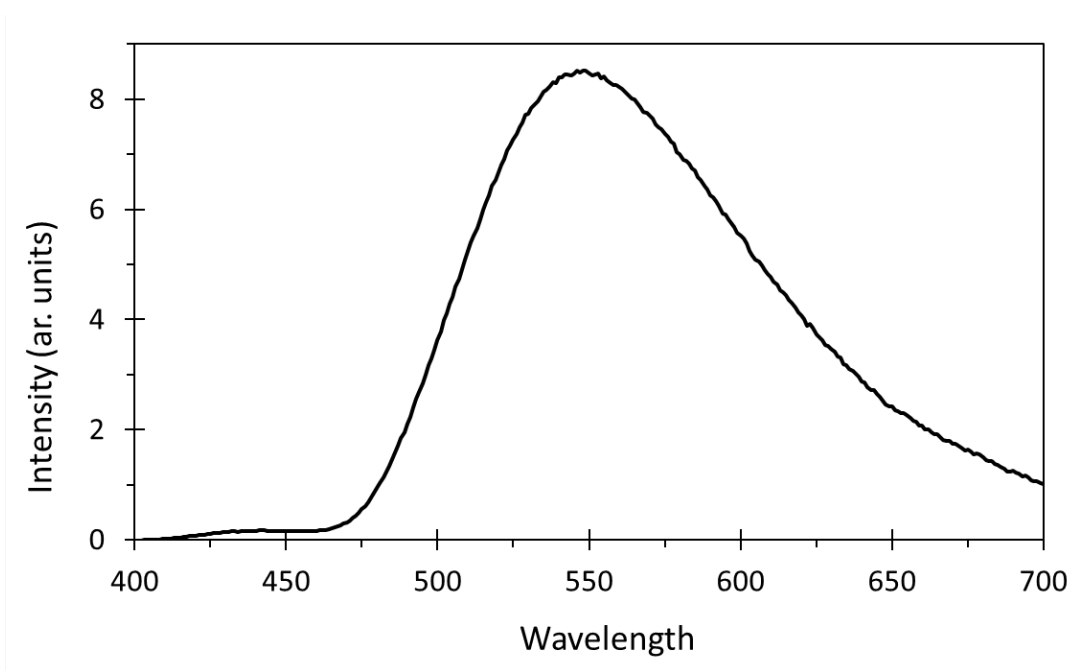


Figure S10. Emission spectrum of a film vapor deposited onto glass substrate of $\text{Si}(\text{bzimpy})_2$.

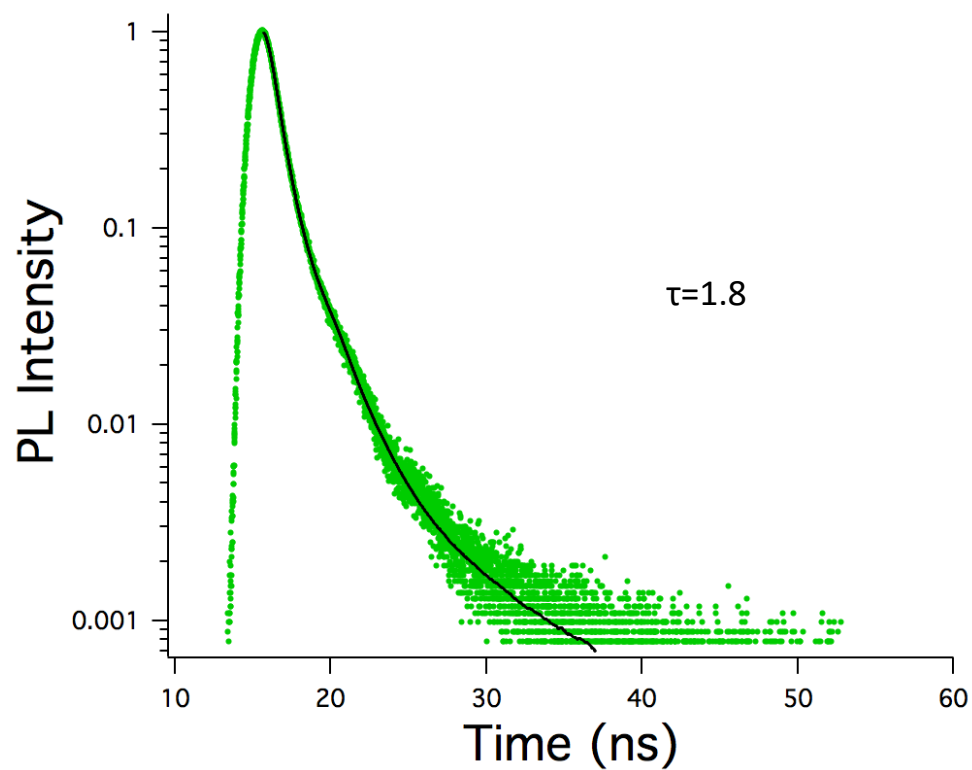


Figure S11. Fluorescence lifetime of $\text{Si}(\text{bzimpy})_2$ film.

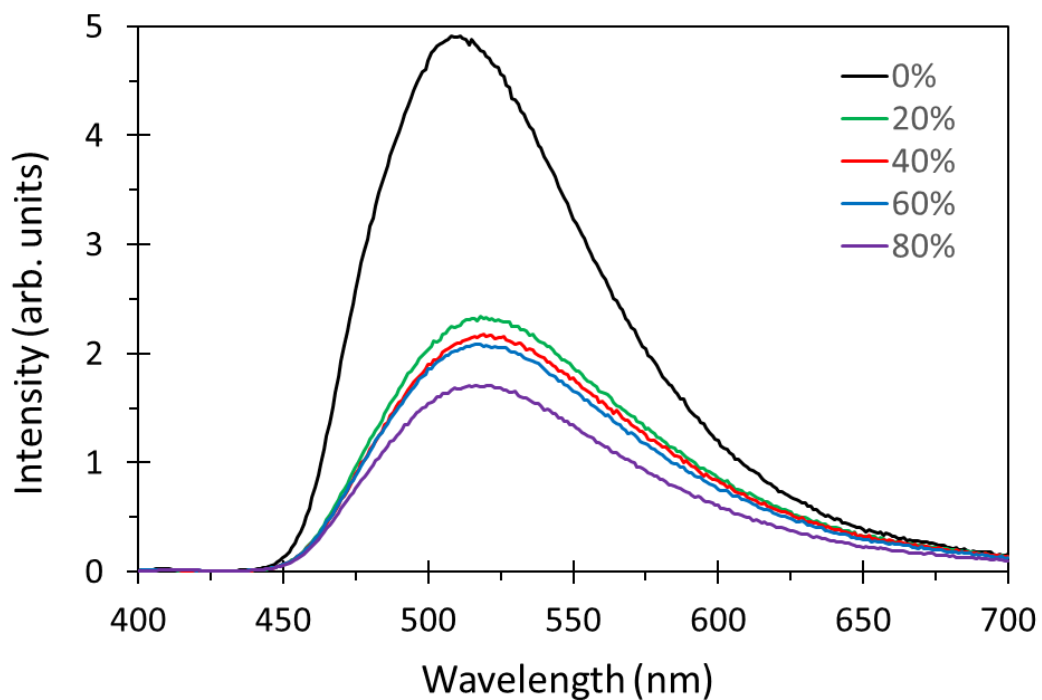


Figure S12. Emission spectra of water/THF solvent mixture **Si(bzimpy)₂**.

Table S1. Quantum yield and lifetime data in THF/H₂O mixture

THF/H ₂ O	QY	τ (ns)	k_{rad} (s ⁻¹)	k_{nr} (s ⁻¹)
100/0	0.5 7	4.3	1.3×10^8	1.0×10^8
80/20	0.2 7	2.9	9.6×10^7	2.6×10^8
60/40	0.2 2	2.5	9.0×10^7	3.1×10^8

40/60	0.2 1	2.4	8.8×10^7	3.3×10^8
20/80	0.1 7	2.3	7.5×10^7	3.5×10^8

Computational Modeling

All calculations were performed using Spartan 2016 (SPARTAN '16 Quantum Mechanics Driver: (Win/64b) Release 1.1.0). The Si(bzimpy)₂ structure was optimized using DFT (B3LYP/6-31G*) in the gas phase. No negative frequencies were observed in the calculated IR spectra confirming a minimum geometry was reached.

The UV-vis spectrum was calculated using time-dependent density functional theory TD-DFT (B3LYP, 6-31G*). The 60 lowest energy transitions were calculated and are listed in **Table S2**. A simulated spectrum was created by adding all of the transitions for each species (after converting to gaussian shaped bands with a standard deviation of $\sigma = 0.38$ eV) using the following equation:^{4,5}

$$\varepsilon(\tilde{\nu}) = \sum_{i=1}^n \varepsilon_i(\tilde{\nu}) = \sum_{i=1}^n \left(1.3062974 \times 10^8 \cdot \frac{f_i}{\sigma} \exp \left[- \left(\frac{\tilde{\nu} - \tilde{\nu}_i}{\sigma} \right)^2 \right] \right)$$

$\tilde{\nu}_i$ is the excitation energy (in wavenumbers) corresponding to the transition

f_i is the oscillator strength of the transition

σ is the standard deviation in wavenumbers

Table S2. Calculated UV-vis transitions for Si(bzimpy)₂ (SPARTAN 2016, TD-DFT, B3LYP/6-31G^{*}).

UV/Vis Allowed Transitions				
transition	nm	strength	MO Component	
1	461.05	0.0143	HOMO -> LUMO	66%
			HOMO-2 -> LUMO	14%
			HOMO-1 -> LUMO+1	11%
2	460.93	0.015	HOMO -> LUMO+1	64%
			HOMO-2 -> LUMO+1	14%
			HOMO-1 -> LUMO	11%
3	446.16	0.018	HOMO-1 -> LUMO	57%
			HOMO-2 -> LUMO	29%
4	445.74	0.0195	HOMO-1 -> LUMO+1	54%
			HOMO-2 -> LUMO+1	31%
5	437.18	0.2503	HOMO-2 -> LUMO	26%
			HOMO-2 -> LUMO+1	23%
			HOMO-1 -> LUMO+1	18%
			HOMO -> LUMO	16%
6	437.08	0.2509	HOMO-2 -> LUMO+1	27%
			HOMO-2 -> LUMO	24%
			HOMO-1 -> LUMO	18%
			HOMO -> LUMO+1	16%
7	433.48	0	HOMO-3 -> LUMO	75%
			HOMO-4 -> LUMO+1	19%
8	432.92	0.0001	HOMO-4 -> LUMO+1	62%
			HOMO-4 -> LUMO	17%
			HOMO-3 -> LUMO+1	13%
9	426.02	0.0075	HOMO-3 -> LUMO+1	38%
			HOMO-4 -> LUMO	27%
			HOMO-4 -> LUMO+1	17%
			HOMO-3 -> LUMO	16%
10	424.87	0	HOMO-4 -> LUMO	54%
			HOMO-3 -> LUMO+1	43%
11	407.38	0	HOMO-5 -> LUMO	87%
12	407.08	0	HOMO-6 -> LUMO+1	86%
13	393.64	0	HOMO-5 -> LUMO+1	32%
			HOMO-6 -> LUMO	30%
			HOMO-1 -> LUMO+2	23%
14	391.41	0.0089	HOMO-6 -> LUMO	37%
			HOMO-5 -> LUMO+1	35%
			HOMO-2 -> LUMO+2	17%
15	390.6	0.001	HOMO-7 -> LUMO	98%
16	390.49	0.001	HOMO-7 -> LUMO+1	98%
17	387.86	0.0049	HOMO -> LUMO+2	96%
18	375.02	0	HOMO-1 -> LUMO+2	60%
			HOMO-2 -> LUMO+3	23%
19	371.07	0.0028	HOMO-3 -> LUMO+2	94%
20	370.8	0.0027	HOMO-4 -> LUMO+2	94%
21	370.52	0.0254	HOMO-2 -> LUMO+2	48%
			HOMO-1 -> LUMO+3	46%
22	364.64	0	HOMO -> LUMO+3	96%
23	353.26	0.1282	HOMO-5 -> LUMO+2	95%
24	353.1	0.13	HOMO-6 -> LUMO+2	95%
25	345.82	0.0122	HOMO-3 -> LUMO+3	95%
26	345.66	0.0124	HOMO-4 -> LUMO+3	95%
27	340.46	0	HOMO-7 -> LUMO+2	96%
28	334.97	0.0002	HOMO-2 -> LUMO+3	75%
			HOMO-1 -> LUMO+2	15%
29	333.02	0.2086	HOMO-5 -> LUMO+3	97%
30	332.89	0.2065	HOMO-6 -> LUMO+3	97%

transition	nm	strength	MO Component	
31	332.03	0.308	HOMO-1 -> LUMO+3	40%
			HOMO-7 -> LUMO+3	26%
			HOMO-2 -> LUMO+2	22%
32	316.68	0.2748	HOMO-7 -> LUMO+3	73%
33	295.54	0.0008	HOMO-9 -> LUMO+1	40%
			HOMO-8 -> LUMO+1	28%
			HOMO-8 -> LUMO	22%
34	295.53	0.0008	HOMO-9 -> LUMO	45%
			HOMO-8 -> LUMO	24%
			HOMO-8 -> LUMO+1	22%
35	294.36	0	HOMO-10 -> LUMO+1	77%
36	294.24	0	HOMO-11 -> LUMO	77%
37	274.66	0.0119	HOMO-8 -> LUMO	44%
			HOMO-9 -> LUMO	42%
38	274.55	0.0119	HOMO-9 -> LUMO+1	48%
			HOMO-8 -> LUMO+1	38%
39	273.67	0.0001	HOMO-10 -> LUMO	49%
			HOMO-11 -> LUMO+1	39%
40	272.68	0.0215	HOMO-11 -> LUMO+1	47%
			HOMO-10 -> LUMO	37%
41	260.34	0.0159	HOMO-12 -> LUMO	96%
42	260.28	0.0161	HOMO-12 -> LUMO+1	96%
43	260.15	0	HOMO-8 -> LUMO+2	75%
44	259.56	0	HOMO-9 -> LUMO+2	73%
			HOMO-8 -> LUMO+3	16%
45	258.89	0.0002	HOMO-10 -> LUMO+2	67%
			HOMO-10 -> LUMO+3	14%
46	258.88	0.0002	HOMO-11 -> LUMO+2	67%
47	248.63	0.0032	HOMO-14 -> LUMO	32%
			HOMO-13 -> LUMO+1	30%
			HOMO-13 -> LUMO	26%
48	248.43	0.0001	HOMO-13 -> LUMO	47%
			HOMO-14 -> LUMO+1	46%
49	248.06	0	HOMO-14 -> LUMO+1	44%
			HOMO-13 -> LUMO	24%
			HOMO-14 -> LUMO	17%
			HOMO-13 -> LUMO+1	15%
50	247.41	0	HOMO-14 -> LUMO	47%
			HOMO-13 -> LUMO+1	46%
51	244.49	0.0348	HOMO-15 -> LUMO	30%
			HOMO-16 -> LUMO	21%
			HOMO-10 -> LUMO+3	12%
			HOMO-1 -> LUMO+4	11%
52	244.42	0.0344	HOMO-15 -> LUMO+1	35%
			HOMO-16 -> LUMO+1	16%
			HOMO-1 -> LUMO+5	12%
			HOMO-11 -> LUMO+3	11%
53	243.39	0.0001	HOMO-8 -> LUMO+3	79%
			HOMO-9 -> LUMO+2	20%
54	242.85	0.0087	HOMO-10 -> LUMO+3	30%
			HOMO-9 -> LUMO+3	20%
			HOMO-15 -> LUMO	11%
			HOMO-1 -> LUMO+4	11%
55	242.81	0.0032	HOMO-9 -> LUMO+3	55%
			HOMO-10 -> LUMO+3	13%
			HOMO-8 -> LUMO+2	11%
56	242.75	0.0088	HOMO-11 -> LUMO+3	39%
			HOMO-1 -> LUMO+5	14%
			HOMO-16 -> LUMO+1	11%
57	241.87	0.0064	HOMO-16 -> LUMO	43%
			HOMO-10 -> LUMO+3	18%
			HOMO-15 -> LUMO	18%
58	241.77	0.0063	HOMO-16 -> LUMO+1	48%
			HOMO-11 -> LUMO+3	18%
			HOMO-15 -> LUMO+1	13%
59	239.62	0.0548	HOMO -> LUMO+4	78%
60	239.56	0.0546	HOMO -> LUMO+5	77%

The combination of the eight transitions with an oscillator strength greater than 0.1 (transitions numbered 5, 6, 23, 24 and 29-32) is qualitatively quite similar to the simulated spectra containing all 60 transitions and similar to the experimental spectrum. In fact, the visible portion of the spectrum is almost entirely attributed to just two transitions. These nearly degenerate, intense transitions numbered 5 and 6 (consisting of transitions from predominantly imidazole based MOs to pyridine based MOs) dominate the low-energy absorbance around 435 nm. Future experiments to tune the optical properties through synthetic modification of the benzimidazole and pyridine moieties is underway.

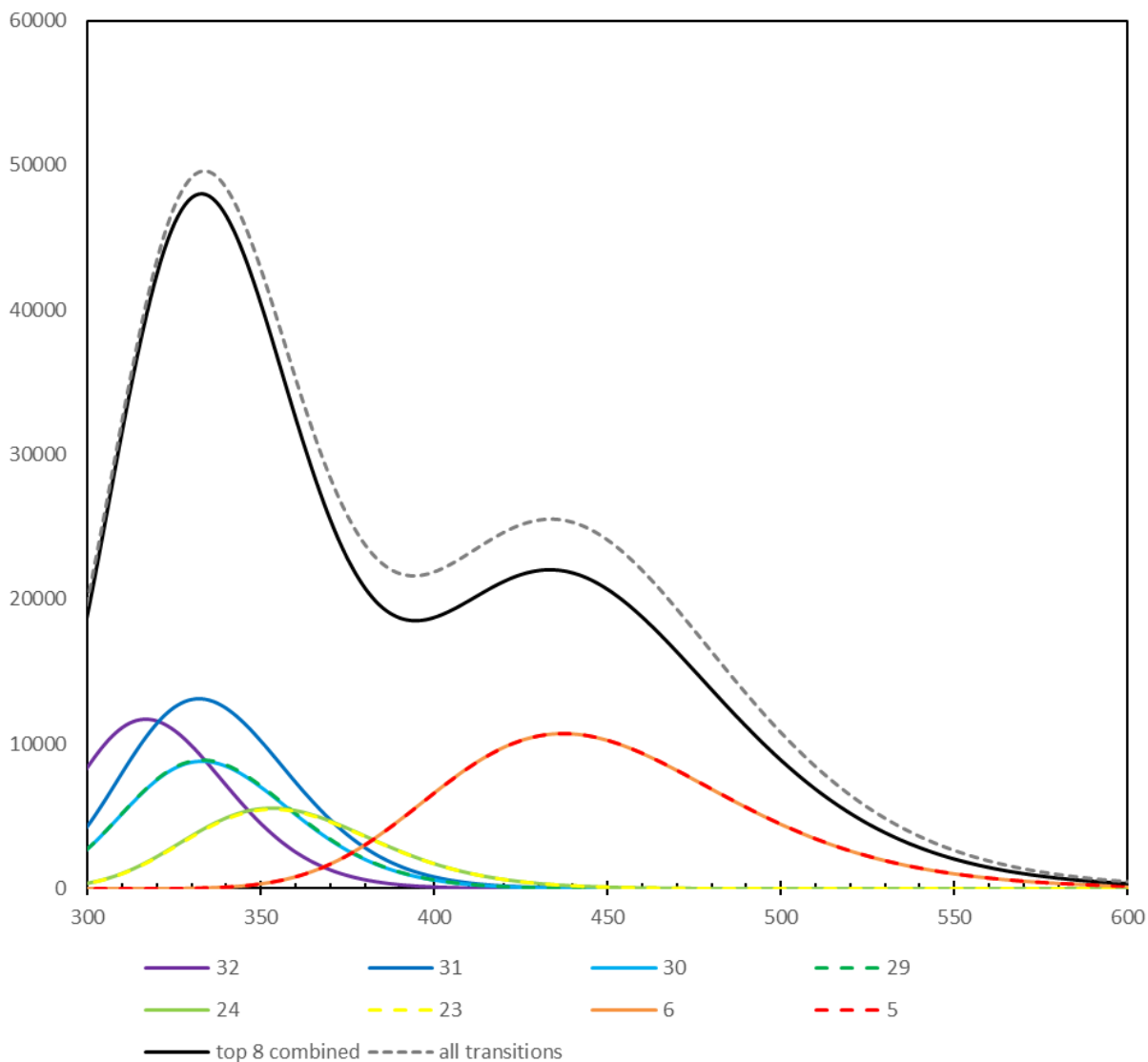


Figure S13. Calculated UV-Vis spectrum constructed from only the eight most intense transitions from Table S2 (solid black line) and spectrum that includes contributions from all 60 lowest energy transitions (dashed gray). Note transitions 5/6, 23/24, and 29/30 are nearly degenerate, equal intensity pairs and overlap in the figure. The numbers correspond to the transition number listed in Table S2.

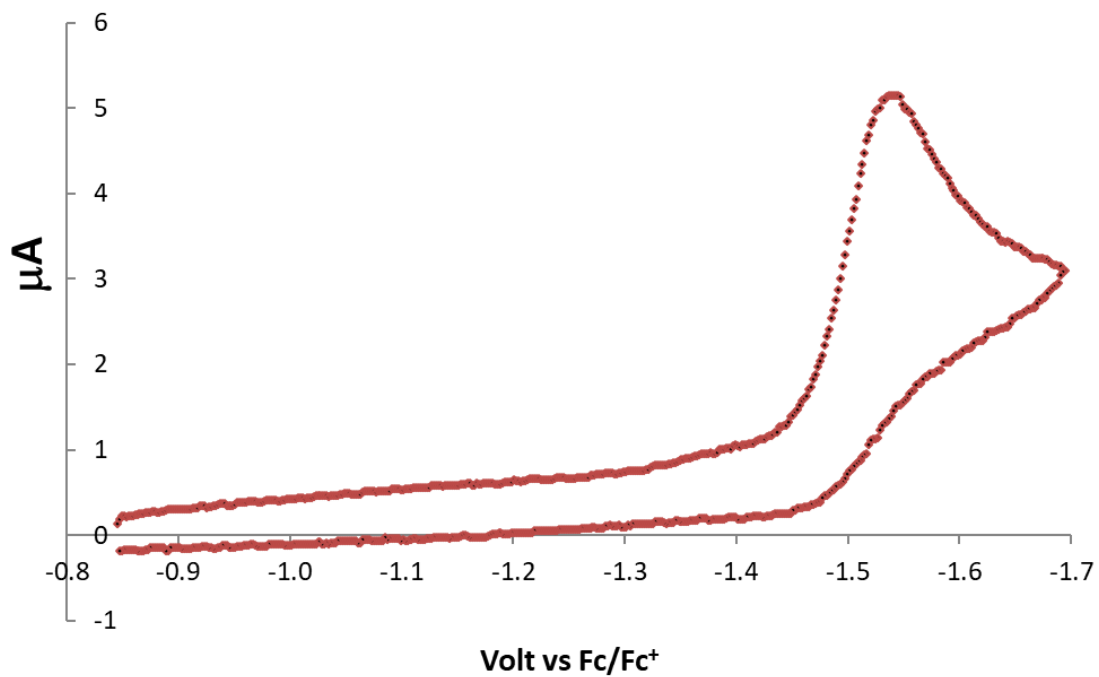


Figure S14. Cyclic voltammogram of **Si(bzimpy)₂** in 0.1M TBAPF₆/CH₃CN solution on a platinum disc working electrode. Scan rate = 200 mV/s.

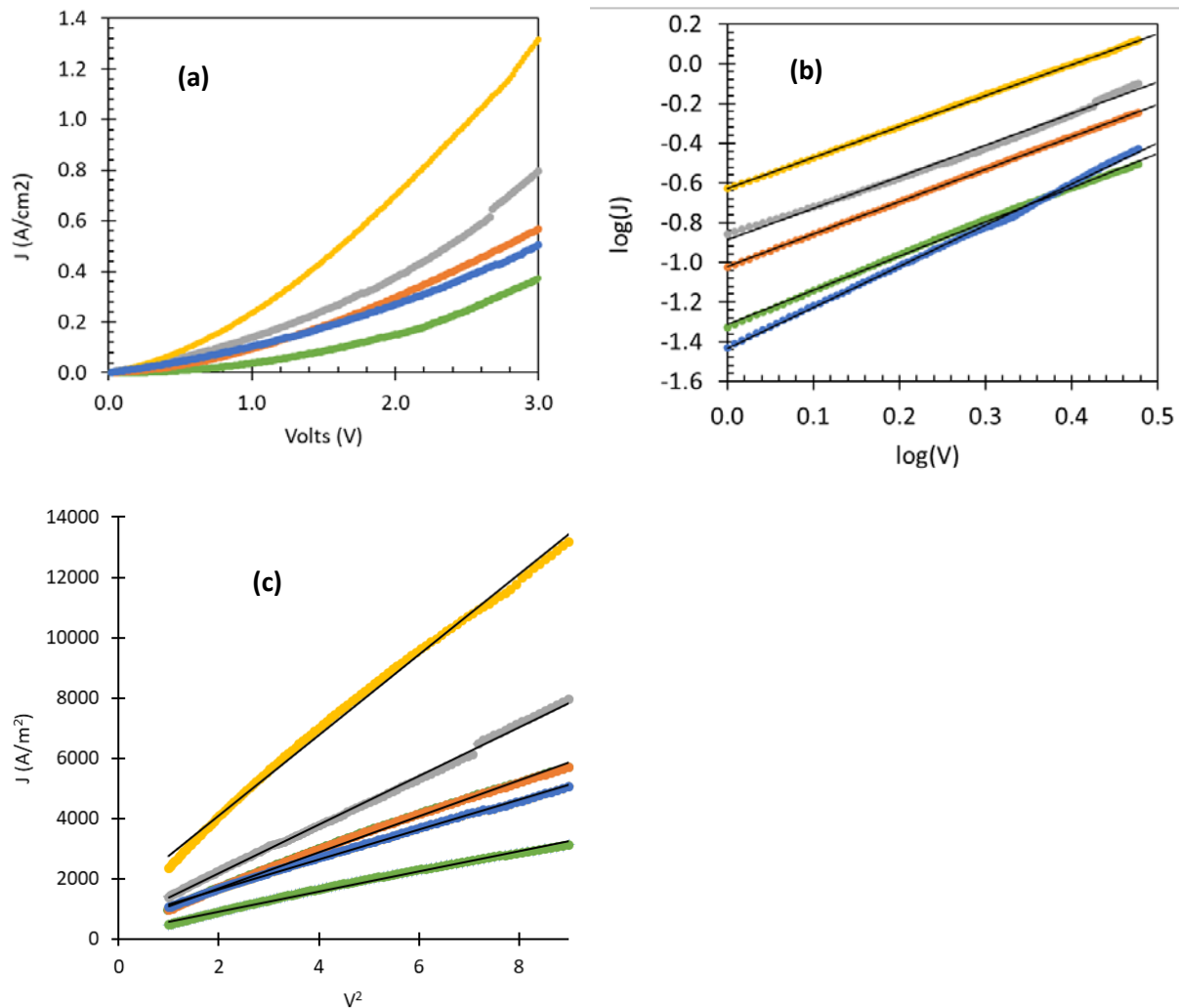


Figure S15. (a) J-V curve of ITO/Si(bzimpy)₂/Al devices. (b) Log(J)-log(V) curve of ITO/Si(bzimpy)₂/Al devices. (c) J-V² curve of ITO/Si(bzimpy)₂/Al devices. Mobilities were calculated from slopes of lines in graph S15c.

Table S3. Summary of graph S15c data and calculated mobility.

color	Sample	Slope (A/V ² m ²)	R ²	mobility (cm ² /Vs)
gold	S 1-2	1.34E+03	0.996	1.18E-04
gray	S 2-4	8.05E+02	0.998	7.07E-05
orange	S 1-1	5.94E+02	0.997	5.21E-05
blue	S 2-5	4.95E+02	0.998	4.34E-05
green	S 2-2	3.33E+02	0.994	2.92E-05

average	6.3E-05
std dev	3.4E-05

References:

1. Rigaku Oxford Diffraction, (2018), CrysAlisPro Software System, version 1.171.38.46, Rigaku Corporation, Oxford, UK.
2. G.M. Sheldrick, *Acta Cryst.* **2008**, *A64*, 112-122.
3. O. V. Dolomanov, L. J. Bourhis, R. J. Gildea, J. A. K. Howard and H. Puschmann, *J. Appl. Cryst.* **2009**, *42*, 339-341.
4. P. J. Stephens and N. Harada, *Chirality*, 2010, **22**, 229-233.
5. B. Peng, S. Q. Yang, L. L. Li, F. Y. Cheng and J. Chen, *J. Chem. Phys.*, 2010, **132**, 034305.